

# GeV and higher energy photon interactions in gamma-ray burst fireballs and surroundings

Soebur Razzaque<sup>1</sup>, Peter Mészáros<sup>1,2,3</sup> and Bing Zhang<sup>1</sup>

<sup>1</sup>*Astronomy & Astrophysics Dpt., Pennsylvania State University, University Park, PA 16802*

<sup>2</sup>*Physics Department, Pennsylvania State University, University Park, PA 16802*

<sup>3</sup>*Institute for Advanced Study, Einstein Drive, Princeton, NJ 08540*

## ABSTRACT

We have calculated the opacities and secondary production mechanisms of high energy photons arising in gamma-ray burst internal shocks, using exact cross-sections for the relevant processes. We find that for reasonable choices of parameters, photons in the range of 10's to 100's of GeV may be emitted in the prompt phase. Photons above this range are subject to electron-positron pair production with fireball photons and would be absent from the spectrum escaping the gamma-ray burst. We find that, in such cases, the fireball becomes optically thin again at ultra-high energies ( $\gtrsim$  PeV). On the other hand, for sufficiently large fireball bulk Lorentz factors, the fireball is optically thin at all energies. Both for  $\gamma\gamma$  self-absorbed and optically thin cases, the escaping high energy photons can interact with infra-red and microwave background photons to produce delayed secondary photons in the GeV-TeV range. These may be observable with GLAST, or at low redshifts with ground-based air Cherenkov telescopes. Detection of the primary prompt spectrum constrains the bulk Lorentz factor, while detection of delayed secondary gamma-rays would provide a consistency check for the primary spectrum and the bulk Lorentz factor as well as constraints on the intergalactic magnetic field strength.

*Subject headings:* gamma rays: bursts—gamma rays: theory—radiation mechanisms: non thermal

## 1. Introduction

GeV photons have been detected from a number of gamma-ray bursts (GRB) (Dingus 2003) with the EGRET detector on the Compton Gamma Ray Observatory. Photons at energies in this range and higher can make pairs via  $\gamma\gamma \rightarrow e^+e^-$  interactions in the GRB fireball, the optical depth being dependent on the bulk Lorentz factor  $\Gamma_b$ , so spectral observations at this energy can provide useful constraints (Baring & Harding 1997; Lithwick & Sari 2001) on this key ingredient of GRB models. In addition, high energy photons which escape  $\gamma\gamma$  absorption in the source can still suffer such interactions far from the source but before reaching the observer, against cosmic infrared

background (CIB) and/or cosmic microwave background (CMB) photons. The electron-positron pairs thus produced can inverse-Compton scatter again on the most numerous CMB photons, giving rise to a delayed secondary spectrum (Plaga 1995; Dai & Lu 2002), which ranges typically up to 100's of GeV.

In this paper we investigate, using the exact cross sections, the high energy interactions of photons produced in a simple GRB internal shock model, as a function of the luminosity, the typical variability timescale and the bulk Lorentz factor. We approximate the original GRB spectrum through an observationally motivated Band function (Band et al. 1993), and calculate the emerging spectrum as a function of the burst parameters. This spectrum is then subjected to interactions with the CIB and CMB, and the shape of the secondary spectrum and its time delay is calculated assuming typical cosmological distances  $z \sim 1$  and various values for the intergalactic magnetic field strength. The pair-production cut-off of the primary spectrum and the delayed secondary spectrum fall, for typical GRB parameters, in the GLAST (Gehrels 1999) energy range, and for a range of intergalactic magnetic field strengths the latter should be detectable by GLAST as well as by the newer generation of air-Cherenkov telescopes (Weekes 2001).

## 2. GRB internal shock model

Denoting with  $U$  the GRB fireball total energy density, after the initial expansion phase the kinetic energy is carried by the baryons since  $m_p \gg m_e$ , where  $m_p$  and  $m_e$  are baryon and lepton masses respectively. Thus,  $U \sim U_p \sim 4n'_p m_p c^2 \Gamma_b^2$ , where  $n'_p$  is the total baryon number density in the comoving fireball frame and  $\Gamma_b$  is the bulk Lorentz factor of the fireball in the observer's frame.<sup>1</sup> Later on, a significant fraction of the fireball's kinetic energy is transferred to leptons, in internal shocks which randomize the relative bulk motion between different portions of the expanding fireball, as well as external shocks when the fireball is decelerated by the external medium. Here we concentrate on the internal shocks, which are thought to be responsible for the usual prompt MeV emission. The fraction of energy transferred to the leptons is given by a parameter  $\varepsilon_e = U_e/U \gg m_e/m_p$ . Charged particles,  $p$  and  $e^+e^-$ , are accelerated in the shocks by interaction with magnetic fields within the GRB fireball. High energy protons and electrons cool mostly due to synchrotron radiation, but the proton cooling time is much longer than that of the electrons, and the prompt  $\gamma$ -ray emission is most likely due to electron synchrotron emission, whose cooling time in the prompt phase (tens of seconds after the trigger) is generally shorter than the dynamical or expansion time.

In this so-called fast cooling case, valid in the internal shocks, most of the electron energy is converted into  $\gamma$ -rays:  $U_e \approx U_\gamma = L_{\gamma,\text{iso}}/(4\pi r_{\text{sh}}^2 c)$ . Here  $r_{\text{sh}} = 2c\delta t\Gamma_b^2$  is the shock radius,  $\delta t$  is the observed variability time scale, and  $L_{\gamma,\text{iso}}$  is the isotropic-equivalent  $\gamma$ -ray luminosity in the

---

<sup>1</sup>We use primed variables in the comoving frame and un-primed variables in the laboratory or observer's frame

observer's frame during the prompt  $\gamma$ -ray emission phase. Neglecting  $e^\pm$  pair formation in the shocks, the total volume number density of leptons and baryons in the fireball (which are the same due to charge neutrality) can be calculated, assuming  $U_p \approx U_\gamma/\varepsilon_e$ , as

$$n'_e \approx n'_p = \frac{L_{\gamma,\text{iso}}/\varepsilon_e}{4\pi r_{\text{sh}}^2 \Gamma_b^2 \bar{\gamma}_p m_p c^3} \quad (1)$$

in the comoving frame. Here  $\bar{\gamma}_p \sim 1$  is the comoving random Lorentz factor acquired by protons in the internal shocks. The magnetic field energy density  $U_B = B^2/8\pi$  can be estimated as

$$B' = \sqrt{\frac{2\varepsilon_B L_{\gamma,\text{iso}}}{\varepsilon_e r_{\text{sh}}^2 c \Gamma_b^2}}, \quad (2)$$

so in the comoving frame  $\varepsilon_B = U_B/U$  is the fraction of the shocked fireball energy that goes into magnetic energy.

The process of Fermi acceleration in the shocks leads to a differential electron and proton volume number density distribution which is a power law in energy,

$$\frac{dN'_{e,p}}{d\gamma'_{e,p}} = \frac{(p-1)n'_{e,p}}{\gamma'_{e,p;\text{min}}} \left( \frac{\gamma'_{e,p}}{\gamma'_{e,p;\text{min}}} \right)^{-p}; \quad \gamma'_{e,p} > \gamma'_{e,p;\text{min}} \quad (3)$$

where

$$\gamma'_{e,\text{min}} \approx \left( \frac{m_p}{m_e} \right) \varepsilon_e \gamma'_{p,\text{min}}; \quad \gamma'_{p,\text{min}} \approx 1 \quad (4)$$

are the minimum Lorentz factors for electrons and protons respectively in the comoving frame. The maximum Lorentz factors are obtained by equating the acceleration time ( $t'_{j,\text{acc}} = Am_j \gamma_j / eB'$ ) of a particle  $j$  to the shorter of the synchrotron cooling time

$$t'_{j;\text{syn}} = \frac{6\pi m_j^3}{\sigma_{\text{Th}} \gamma_j m_e^2 B'^2} \quad (5)$$

and the dynamic time ( $\delta t \Gamma_b$ ) in the comoving frame. Electrons cool faster, by synchrotron radiation, than the dynamic time and the maximum electron Lorentz factor is

$$\begin{aligned} \gamma'_{e,\text{max}} &= \sqrt{\frac{6\pi e}{A\sigma_{\text{Th}} B'}} \\ &\approx 2.2 \times 10^6 A_1^{-1/2} L_{\gamma,52}^{-1/4} \varepsilon_{e,-1}^{1/4} \varepsilon_{B,-1}^{-1/4} \delta t_{-2}^{1/2} \Gamma_{b,2.5}^{5/2} \end{aligned} \quad (6)$$

in the comoving frame. Here we have chosen  $L_{\gamma,\text{iso}} = 10^{52} L_{\gamma,52}$  erg/s,  $\varepsilon_e = 10^{-1} \varepsilon_{e,-1}$ ,  $\varepsilon_B = 10^{-1} \varepsilon_{B,-1}$ ,  $\delta t = 10^{-2} \delta t_{-2}$  s,  $A = 10A_1$  and  $\Gamma_b = 10^{2.5} \Gamma_{b,2.5}$ .

The observed  $\gamma$ -ray spectrum from the GRB prompt emission can be approximated by the phenomenological Band function in the high energy range as  $\sim \varepsilon_\gamma^{-\alpha}$  above the synchrotron peak

energy  $\epsilon_{\gamma,\text{pk}}$ , which is typically a few hundred keV. For observed cases of  $\alpha > 2$ , most of the  $\gamma$ -ray energy is concentrated near  $\epsilon_{\gamma,\text{pk}}$  and one can roughly estimate the peak volume number density of photons in the fireball as

$$n'_\gamma = \frac{L_{\gamma,\text{iso}}}{4\pi r_{\text{sh}}^2 c \Gamma_b \epsilon_{\gamma,\text{pk}}} \quad (7)$$

in the comoving frame. Below the synchrotron peak energy the Band spectrum is  $\sim \epsilon_\gamma^{-1}$  and the total number density of photons in equation (7) increases only logarithmically.

Low energy photons are expected to be absorbed by fireball electrons in the presence of a magnetic field by the synchrotron self-absorption mechanism below a photon energy of

$$\begin{aligned} \epsilon_{\gamma,\text{ssa}} &= \Gamma_b \left[ \frac{\pi(-1)}{2} \Gamma\left(\frac{p}{4} + \frac{11}{6}\right) \Gamma\left(\frac{p}{4} + \frac{1}{6}\right) \gamma_{e,\text{min}}^{p-1} n'_{e,r'_{\text{sh}}} \right]^{\frac{2}{p+4}} \left[ 3^{p+1} \frac{q^{p+6} (B' \sin \theta)^{p+2}}{m_e^{p+4}} \right]^{\frac{1}{p+4}} \\ &\approx \begin{cases} 11 L_{\gamma,52}^{2/3} \epsilon_{e,-1}^{-2/3} \epsilon_{B,-1}^{1/3} \delta t_{-2}^{-1} \Gamma_{b,2.5}^{-8/3} \text{ keV}; & p = 2 \\ 13 L_{\gamma,52}^{17/26} \epsilon_{e,-1}^{-17/26} \epsilon_{B,-1}^{9/26} \delta t_{-2}^{-1} \Gamma_{b,2.5}^{-34/13} \text{ keV}; & p = 2.5 \\ 14 L_{\gamma,52}^{9/14} \epsilon_{e,-1}^{-9/14} \epsilon_{B,-1}^{5/14} \delta t_{-2}^{-1} \Gamma_{b,2.5}^{-18/7} \text{ keV}; & p = 3 \end{cases} \quad (8) \end{aligned}$$

in the observer's frame. Here we have estimated  $\epsilon_{\gamma,\text{ssa}}$  for power law indices in equation (3) of  $p = 2, 2.5, 3$  (top to bottom in the equation above). Observed GRB spectra, fitted by a Band function, do not correspond in a straightforward manner to a theoretical synchrotron spectrum from a one-zone region with some power-law index  $p$ , especially in the fast-cooling regime. However, the usual Band function values can arise as a result of the superposition of many shocks, each giving rise to a power law energy distribution with index  $2 \lesssim p \lesssim 3$ . In our calculation, we assume the nominal Band fit values for the resulting photon spectrum, and we use a nominal reference value for the absorption energy of  $\epsilon_{\gamma,\text{ssa}} = 10\epsilon_{\gamma,1}$  keV, which is more than an order of magnitude below the observed synchrotron peak energy of  $\epsilon_{\gamma,\text{pk}} = 500\epsilon_{\gamma,2.7}$  keV.

### 3. High energy photon interactions and internal attenuation

Observation of high energy photons from the GRB fireball is mainly limited by the opacity of two photon annihilation into an electron-positron pair ( $e^\pm$ ). The cross-section for  $\gamma\gamma \rightarrow e^\pm$  in the non-relativistic (NR) and extremely relativistic (ER) cases is given by Jauch & Rohrlich (1955) as

$$\begin{aligned} \sigma_{\gamma\gamma}^{\text{NR}}(\omega) &= \frac{3}{8} \sigma_{\text{Th}} \sqrt{1 - \frac{m_e^2 c^4}{\omega^2}} \\ \sigma_{\gamma\gamma}^{\text{ER}}(\omega) &= \frac{3}{8} \sigma_{\text{Th}} \frac{m_e^2 c^4}{\omega^2} \left( \ln \frac{2\omega}{m_e c^2} - 1 \right) \end{aligned} \quad (9)$$

where  $\omega$  is the photon energy in the center of mass frame. The observed photon energy ( $E_\gamma$ ) above the threshold for pair production with photons at an energy  $\epsilon_\gamma$  must satisfy the condition  $\omega > m_e c^2$

or  $E_\gamma \gtrsim E_{\gamma,\text{th}} = m_e^2 c^4 \Gamma_b^2 / 2\epsilon_\gamma$ . Observation of photons of a maximum energy  $\epsilon_{\gamma,\text{max}} > E_{\gamma,\text{th}}$  may therefore be used to put a limit on  $\Gamma_b$  if the corresponding optical depth is unity. Photons below  $E_{\gamma,\text{th}}$  may escape from the fireball (provided no other interaction becomes important) even though they might interact with photons from the high energy tail of the Band function, but the relevant optical depth is less than unity because of a much lower photon density, at that energy, than in equation (7).

For a given  $\Gamma_b$  and  $\delta t$ , the lower limit threshold of the  $\gamma\gamma$  absorption energy range within the source can be found from the pair production threshold energy with peak synchrotron photons of energy  $\epsilon_{\gamma,\text{pk}}$  as

$$E_{\gamma,\text{pk,th}} = \frac{m_e^2 c^4 \Gamma_b^2}{2\epsilon_{\gamma,\text{pk}}} \approx 26 \Gamma_{b,2.5}^2 \epsilon_{\gamma,2.7}^{-1} \text{ GeV} \quad (10)$$

in the observer’s frame, for the present choice of parameters. The total volume number density of photons and hence the  $\gamma\gamma$  optical depth in the fireball increases slowly as the photon energy decreases from  $\epsilon_{\gamma,\text{pk}}$  to  $\epsilon_{\gamma,\text{ssa}}$ . High energy photons in the energy range capable of producing pairs with fireball photons in the energy range  $\epsilon_{\gamma,\text{pk}} - \epsilon_{\gamma,\text{ssa}}$  are absent in the spectrum escaping from the source. Ultra high energy photons, however, may escape the GRB fireball as the pair production cross-section, in the ER limit in equation (9), decreases with increasing photon energy and so does the optical depth. Ultra high energy primary photons will appear again above this “thinning” energy. This energy can be found, roughly, from the optical depth corresponding to the  $\gamma\gamma$  cross-section with photons at self absorption energy ( $\epsilon_{\gamma,\text{ssa}}$ ) in the ER limit in equation (9) as

$$\begin{aligned} E_{\gamma,\text{thin}} &= \frac{3\Lambda}{64\pi} \frac{L_{\gamma,\text{iso}} \sigma_{\text{Th}} m_e^2 c^2}{\Gamma^2 \delta t \epsilon_{\gamma,\text{ssa}}^2} \\ &\approx 2 \times 10^7 \Lambda_3 L_{\gamma,52} \Gamma_{b,2.5}^{-2} \delta t_{-2}^{-1} \epsilon_{\gamma,1}^{-2} \text{ GeV} \end{aligned} \quad (11)$$

where  $\Lambda = \ln(2\sqrt{2\epsilon_{\gamma,\text{ssa}} E_\gamma} / m_e \Gamma_b) - 1 \sim 3\Lambda_3$ , for the same parameters used in equation (11).

We calculate the high energy photon interactions with other fireball photons and electrons using the exact cross-section formulae (Jauch & Rohrlich 1955). The opacities of high energy photons are plotted in Figure 1, as a function of observed energy ( $E_\gamma$ ), due to electron Compton scattering,  $e^\pm$  pair production with electrons ( $e\gamma \rightarrow e^\pm$ ) and by  $\gamma\gamma$  interactions, dominantly, with fireball photons in the energy range  $\epsilon_{\gamma,\text{ssa}} - \epsilon_{\gamma,\text{pk}}$ . The cross-section for the  $e\gamma \rightarrow e^\pm$  process is given by Jauch & Rohrlich (1955) as

$$\begin{aligned} \sigma_{e\gamma}^{\text{NR}}(E'_\gamma) &= 2.25 \times 10^{-3} \frac{\alpha}{\pi} \sigma_{\text{Th}} \left( \frac{E'_\gamma}{m_e c^2} - 4 \right) \\ \sigma_{e\gamma}^{\text{ER}}(E'_\gamma) &= \frac{3\alpha}{8\pi} \sigma_{\text{Th}} \left( \frac{28}{9} \ln \frac{2E'_\gamma}{m_e c^2} - \frac{218}{27} \right) \end{aligned} \quad (12)$$

in the non-relativistic and extreme relativistic limits respectively. Here  $E'_\gamma$  is the photon energy in the comoving frame. The flat region, in Figure 1, for the  $\gamma\gamma$  pair creation curves above  $E_{\gamma,\text{pk,th}}$

corresponds to a change in the target photon energy from  $\epsilon_{\gamma,\text{pk}}$  to  $\epsilon_{\gamma,\text{ssa}}$  and a slow increase of the total target photon number density  $n'_\gamma$ , in equation (7), accordingly.

We have plotted the boundaries of the optically thin and thick regions for high energy photon emission from GRB internal shocks in Figure 2, for different choice of parameters  $L_\gamma$ ,  $\epsilon_{\gamma,\text{pk}}$  and  $\delta t$ . Note that for certain parameter values, e.g.  $L_{\gamma,\text{iso}} = 10^{51}$  erg/s,  $\delta t = 0.1$  s and  $\epsilon_{\gamma,\text{pk}} = 0.5$  MeV; or  $L_{\gamma,\text{iso}} = 10^{52}$  erg/s,  $\delta t = 1$  s and  $\epsilon_{\gamma,\text{pk}} = 1$  MeV, the GRB fireball is optically thin to photons of all energies above  $\Gamma_b \approx 775$  or 676 respectively.

Extra complications can arise due to increased  $e^\pm$  pairs produced in the fireball by  $\gamma\gamma$  interactions by high energy photons, which can affect the photon opacities plotted in Figure 1. This is a complex problem, requiring a numerical treatment (Pe'er & Waxman 2003). Here we use an approximate treatment, using a pair formation rate in the comoving frame of  $c\sigma_{\gamma\gamma}(\epsilon'_\gamma)dN'_{\gamma,i}/d\epsilon'_\gamma$  to estimate the total number of  $e^\pm$  pairs created by an incident (denoted by “i”) high energy photon. The differential volume number density of incident high energy photons capable of producing pairs, as a function of energy, can be estimated using the Band spectrum and equation (7) as

$$\frac{dN'_{\gamma,i}}{d\epsilon'_\gamma} \approx \frac{\alpha - 1}{\epsilon'_{\gamma,\text{pk}}} \frac{n'_\gamma}{(\epsilon'_\gamma/\epsilon'_{\gamma,\text{pk}})^\alpha}; \quad \epsilon'_\gamma \gtrsim \epsilon'_{\gamma,\text{pk,th}}. \quad (13)$$

Here  $\epsilon'_{\gamma,\text{pk,th}}$  is the comoving threshold energy for pair production which is similar to the threshold energy in equation (10) in the case of synchrotron peak photons as targets. The target (denoted by “t”) photon number density, in general, may have a different energy distribution  $dN'_{\gamma,t}/dE'_\gamma$ . The total volume number density of pairs created in the fireball is thus

$$n'_\pm = c\delta t\Gamma \int_{\epsilon'_{\gamma,\text{th}}}^{\epsilon'_{\gamma,\text{max}}} d\epsilon'_\gamma \frac{dN'_{\gamma,i}}{d\epsilon'_\gamma} \int_{\epsilon'_{\gamma,\text{th}}}^{\epsilon'_{\gamma,\text{max}}} dE'_\gamma \sigma_{\gamma\gamma} \left( \sqrt{2\epsilon'_\gamma E'_\gamma} \right) \frac{dN'_{\gamma,t}}{dE'_\gamma}, \quad (14)$$

where  $\epsilon'_{\gamma,\text{max}} \approx \gamma'_{e,\text{max}} m_e c^2$  is defined in equation (6), and  $\epsilon'_{\gamma,\text{th}} = m_e^2 c^4 / 2E'_\gamma$ . For this estimate, we approximate the  $\gamma\gamma$  cross-section as  $\sigma_{\gamma\gamma} \approx (3/8)\sigma_{\text{Th}}$  at  $e^\pm$  pair production threshold with peak synchrotron photons ( $\epsilon_{\gamma,\text{pk}}$ ). This leads to a simplified expression for the total volume number density of pairs created in the fireball by integrating over the photon energy distribution above  $\epsilon'_{\gamma,\text{th}}$ ,

$$n'_\pm = \frac{3}{8}\sigma_{\text{Th}} \frac{c\delta t}{\alpha - 1} \Gamma_b n_\gamma'^2 \left( \frac{2\epsilon_{\gamma,\text{pk}}^2}{m_e^2 c^4 \Gamma_b^2} \right)^{\alpha-1}. \quad (15)$$

The total number density of target photons in equation (7) increases by a factor  $\sim \ln(\epsilon_{\gamma,\text{pk}}/\epsilon_{\gamma,\text{ssa}})$  as the target photon energy decreases from  $\epsilon_{\gamma,\text{pk}}$  to  $\epsilon_{\gamma,\text{ssa}}$  in case of  $\alpha = 2$ . However, one needs incident photons of energy much higher than  $\epsilon_{\gamma,\text{pk}}$  to produce  $e^\pm$  pairs with photons at  $\epsilon_{\gamma,\text{ssa}}$ , and the incident number decreases  $\propto E'_\gamma{}^{-\alpha}$ . Thus equation (15) is estimated for targets which are at threshold with incident photons of energy  $\geq \epsilon_{\gamma,\text{pk}}$ . We can express the secondary pair density as

the ratio to the initial electron density in the fireball,

$$\begin{aligned} \frac{n'_{\pm}}{n'_e} &= \frac{3}{128\pi} \frac{\sigma_{\text{Th}}}{\alpha - 1} \frac{L_{\gamma,\text{iso}} \varepsilon_e m_p}{\Gamma_b^3 \delta t \varepsilon_{\gamma,\text{pk}}^2} \left( \frac{2\varepsilon_{\gamma,\text{pk}}^2}{m_e^2 c^4 \Gamma_b^2} \right)^{\alpha-1} \\ &\approx \begin{cases} 786 L_{\gamma,52} \varepsilon_{e,-1} \delta t_{-2}^{-1} \Gamma_{b,2.5}^{-5}; & \alpha = 2 \\ 2.3 L_{\gamma,52} \varepsilon_{e,-1} \delta t_{-2}^{-1} \varepsilon_{\gamma,2.7} \Gamma_{b,2.5}^{-6}; & \alpha = 2.5 \\ 0.008 L_{\gamma,52} \varepsilon_{e,-1} \delta t_{-2}^{-1} \varepsilon_{\gamma,2.7}^2 \Gamma_{b,2.5}^{-7}; & \alpha = 3 \end{cases} \end{aligned} \quad (16)$$

using equation (1).

Shock accelerated high energy electrons may also produce  $e^{\pm}$  pairs interacting with synchrotron photons ( $e\gamma \rightarrow ee^{\pm}$ ). (The cross-section for this process is given by equation (12) with the replacement  $E'_{\gamma}/m_e \rightarrow \gamma'_e E'_{\gamma}/m_e$ ). However, the number of secondary pairs produced in this case is negligible compared to the initial lepton number density because of the lower number density of high energy incident electrons.

The secondary pairs can annihilate with themselves or with the leptons originally carried in the fireball,  $e^+e^- \rightarrow \gamma\gamma$ , if the number density of pairs increases substantially. The cross-section for this process is (Jauch & Rohrlich 1955)

$$\sigma_{e^{\pm}} = \frac{3}{8} \frac{\sigma_{\text{Th}}}{\gamma'_e (\gamma'_e + 1)} \left[ \left( \gamma'_e + 4 + \frac{1}{\gamma'_e} \right) \ln \left( \gamma'_e + \sqrt{\gamma'^2_e - 1} \right) - (\gamma'_e + 3) \right]. \quad (17)$$

Because of a decreasing cross-section with energy, low energy  $e^{\pm}$  pairs annihilate faster. The annihilation time for an incident electron can be estimated as  $t'_{\text{ann}} = 1/(c\sigma_{e^{\pm}} n'_{\pm})$  in the comoving frame. However, synchrotron cooling is even faster and the ratio of pair annihilation time and synchrotron cooling time, for example at  $\gamma'_e = 5$  (where the electron is still relativistic and synchrotron loss formula applies),  $\Gamma_b = 10^{2.5}$ ,  $\delta t = 0.01$  s and in  $\alpha = 2$  case in equation (16), is  $t'_{e,\text{syn}}/t'_{\text{ann}} \approx 0.1$  using equations (5) and (17). This ratio decreases at higher energy. Hence electrons lose most of their energy to synchrotron photons within a dynamical time  $\delta t \Gamma_b$  in the comoving frame. As a result, secondary pairs produced in the fireball cool down to nonrelativistic values and drift along roughly with the bulk Lorentz factor  $\Gamma_b$ . We consider here situations where the secondary pair density, equation (16), is at most comparable to the original fireball lepton density, in which case the scattering depth is not substantially changed, and any photons from annihilation of cold pairs lead to higher generation pairs whose number similarly does not affect the scattering optical depth. We note that in the Thomson limit, inverse Compton (IC) cooling time is of the same order as the synchrotron cooling time  $t'_{e,\text{IC}}/t'_{e,\text{syn}} \approx \varepsilon_e/\varepsilon_B$  with an increasing value at higher energy and in the Klein-Nishina limit.

#### 4. High energy photon spectrum and interaction with the diffuse background

Using the phenomenological Band function spectrum for the intrinsic high energy photon flux from the GRB, the spectrum that would reach the observer after taking into account in-source  $\gamma\gamma$

attenuation at a luminosity distance  $D_L$  is

$$\frac{d^2 N_\gamma}{d\epsilon_\gamma dt} = \frac{(\alpha - 1)L_{\gamma,\text{iso}}}{4\pi D_L^2 \epsilon_{\gamma,\text{pk}}^2} \left( \frac{\epsilon_\gamma}{\epsilon_{\gamma,\text{pk}}} \right)^{-\alpha} e^{-\tau_{\gamma\gamma,\text{grb}}(\epsilon_\gamma)}; \quad \epsilon_\gamma \gtrsim \epsilon_{\gamma,\text{pk}} \quad (18)$$

where  $\tau_{\gamma\gamma,\text{grb}}(\epsilon_\gamma)$  is the  $e^\pm$  pair production optical depth (see in Figure 1) in the GRB fireball. The high optical depth in the fireball, however, reduces substantially the ultra-high energy photon flux above the energy  $E_{\gamma,\text{pk,th}}$  given in equation (10) and below the energy  $E_{\gamma,\text{thin}}$  given in equation (11), while for some parameters the GRB is in the region of Figure 2 where the escaping spectrum is optically thin at all energies. Here we consider high energy photon emission from the GRB fireball for two cases. One is an example where the escaping spectrum is optically thin at all energies (e.g.  $L_{\gamma,\text{iso}} = 10^{52}$  erg/s,  $\delta t = 1$  s,  $\epsilon_{\gamma,\text{pk}} = 1$  MeV and  $\Gamma_b = 10^{2.9}$  in Figure 2). The other example is a case when the fireball is opaque to photons in an energy range between  $E_{\gamma,\text{pk,th}}$  and  $E_{\gamma,\text{thin}}$  (e.g.  $L_{\gamma,\text{iso}} = 10^{52}$  erg/s,  $\delta t = 0.1$  s and  $\epsilon_{\gamma,\text{pk}} = 0.5$  MeV and  $\Gamma_b = 10^{2.5}$ ).

For typical GRB locations at redshift  $z = 1$ , most high energy photons above  $\sim 70$  GeV produce  $e^\pm$  pairs (Salamon & Stecker 1998), reaching an energy up to  $\sim m_e \gamma_{e,\text{max}}/2$ , due to  $\gamma\gamma$  interactions with cosmic infra-red background (CIB) photons (in the  $\sim 100$  GeV-TeV range), and cosmic microwave background (CMB) photons (in the PeV range). These high energy pairs, in turn, cause delayed high energy photon emission by inverse Compton (IC) scattering of CMB photons (Dai & Lu 2002). Here we follow the treatment of Dai et al. (2002) to calculate the delayed high energy photon spectrum in the GeV-TeV range.

The corresponding time integrated flux of electrons (and positrons) from high energy GRB photons interacting with CIB and CMB photons is

$$\begin{aligned} \frac{dN_e}{d\gamma_e} &= \frac{L_{\gamma,\text{iso}}\delta t}{2\pi D_L^2} \frac{\alpha - 1}{(2m_e)^{\alpha-1}} \frac{\epsilon_{\gamma,\text{pk}}^{\alpha-2}}{\gamma_e^\alpha} e^{-\tau_{\gamma\gamma,\text{grb}}(2\gamma_e m_e)} \\ &\times \left[ 1 - e^{-\tau_{\gamma\gamma,\text{bkg}}(2\gamma_e m_e)} \right] \Theta \left( \frac{m_e}{4\epsilon_{\gamma,\text{cib;cmb}}} \lesssim \gamma_e \lesssim \frac{\gamma_{e,\text{max}}}{2} \right), \end{aligned} \quad (19)$$

where  $\Theta$  is a step function. We have assumed that each electron and positron of the  $e^\pm$  pair share 1/2 the photon energy, i.e.  $\gamma_e = \epsilon_\gamma/2m_e$ . We calculate the pair production optical depth with background photons (CIB and CMB) at threshold ( $2\epsilon_\gamma\epsilon_{\gamma,\text{cib;cmb}} = m_e^2$ ) as

$$\tau_{\gamma\gamma,\text{bkg}}(\epsilon_\gamma) = \max\{n_{\text{cib}}(m_e^2/2\epsilon_\gamma), n_{\text{cmb}}(m_e^2/2\epsilon_\gamma)\} \times (3/8)\sigma_{\text{Th}}D_L \quad (20)$$

The total number density of CIB photons is fitted from the intensity  $\mathcal{I}$  ( $\text{W}\cdot\text{m}^{-2}\text{sr}^{-1}$ ) given in Malkan & Stecker (2001) as

$$n_{\text{cib}}(\epsilon_{\gamma,\text{cib}}) = \frac{4\pi\mathcal{I}(1+z)^3}{c\epsilon_{\gamma,\text{cib}}}. \quad (21)$$

The CMB photons, on the other hand, have a black body distribution peaking at an energy of  $2.7(1+z)$  K and a total volume number density  $\propto (1+z)^3$ .

The secondary electrons in equation (19) are cooled by IC scattering on CMB photons on a timescale  $t_{\text{IC}}(\gamma_e) = 3m_e c / (4\gamma_e \sigma_{\text{Th}} u_{\text{cmb}}) \approx 7.3 \times 10^{13} (\gamma_e / 10^6)^{-1}$  s in the local rest frame (Dai et al. 2002), where  $u_{\text{cmb}}$  is the local black body CMB photon energy density. The total integrated, first generation, IC photon spectrum in the observer’s frame, convolving the electron spectrum with the IC spectrum from a single electron in the Thomson limit (Blumenthal & Gould 1970), is then

$$\begin{aligned} \frac{d^2 N_{\text{delayed IC}}}{dt dE_\gamma} &= \int \int d\gamma_e \frac{dN_e}{d\gamma_e} \frac{d^2 N_\gamma}{dt dE_\gamma} \\ &= \frac{3\sigma_{\text{Th}} c}{32\pi D_L^2} \frac{(\alpha - 1)\epsilon_{\gamma, \text{pk}}^{\alpha-2}}{(2m_e)^{\alpha-1}} L_{\gamma, \text{iso}} t_{\text{grb}} \exp[-\tau_{\gamma\gamma, \text{bkg}}(E_\gamma)] \\ &\quad \times \int d\gamma_e \gamma_e^{-(\alpha+4)} \exp[-\tau_{\gamma\gamma, \text{grb}}(2\gamma_e m_e)] (1 - \exp[-\tau_{\gamma\gamma, \text{bkg}}(2m_e \gamma_e)]) \frac{t_{\text{IC}}(\gamma_e)}{\Delta t(\gamma_e)} \\ &\quad \times \int d\epsilon_{\gamma, \text{cmb}} \frac{n_{\text{cmb}}(\epsilon_{\gamma, \text{cmb}})}{\epsilon_{\gamma, \text{cmb}}^2} \left[ 2E_\gamma \ln \frac{E_\gamma}{4\gamma_e^2 \epsilon_{\gamma, \text{cmb}}} + E_\gamma + 4\gamma_e^2 \epsilon_{\gamma, \text{cmb}} - \frac{E_\gamma^2}{2\gamma_e^2 \epsilon_{\gamma, \text{cmb}}} \right] \end{aligned} \quad (22)$$

Here the integration over  $\gamma_e$  ranges from  $\gamma_{e, \text{min}} = \max\{m_e / (4\epsilon_{\gamma, \text{cmb}}), \sqrt{E_\gamma / \epsilon_{\gamma, \text{cmb}}} / 2\}$  to  $\sim \gamma_{e, \text{max}} / 2$  where  $\gamma_{e, \text{max}}$  is the maximum electron energy in equation (6). The maximum time scale for delayed emission is  $\Delta t(\gamma_e) = \max\{\Delta t_{\text{IC}}, \Delta t_A, \Delta t_B, t_{\text{grb}}\}$ , where  $\Delta t_{\text{IC}}(\gamma_e) = t_{\text{IC}} / (2\gamma_e^2)$  is the IC cooling time;  $\Delta t_A(\gamma_e) = \lambda_{\gamma\gamma, \text{bkg}} / (2\gamma_e^2 c)$  is the angular spreading time;  $\Delta t_B(\gamma_e) = t_{\text{IC}} \theta_B^2 / 2$  is the delay time due to magnetic deflection, all evaluated in the observer’s frame; and  $\lambda_{\gamma\gamma, \text{bkg}} = (\max\{n_{\text{cib}}, n_{\text{cmb}}\} (3/8) \sigma_{\text{Th}})^{-1}$  is the pair production mean free path against background photons. For  $10^{-20} B_{\text{IG}, -20}$  G inter galactic (IG) magnetic field, the deflection angle, for  $\theta_B \ll 1$ , is  $\theta_B \approx \lambda_e / R_g \approx 1.3 \times 10^{-5} (\gamma_e / 10^6)^{-2} (B_{\text{IG}, -20})^2$ , where  $R_g = \gamma_e m_e c^2 / (eB)$  is the Larmor gyroradius of the electron. We have plotted different time scales as a function of secondary pair Lorentz factor ( $\gamma_e$ ) in Figure 3 for  $t_{\text{grb}} = 50$  s and several IG magnetic field values, at  $D_L = 10^{28}$  cm corresponding to redshift  $z \simeq 1$  in an  $\Omega_m = 0.3$ ,  $\Omega_\Lambda = 0.7$  and  $H_o = 75$  km s $^{-1}$  Mpc $^{-1}$  cosmology.

We used two parameter sets ( $L_{\gamma, \text{iso}} = 10^{52}$  erg/s,  $\delta t = 1$  s,  $\epsilon_{\gamma, \text{pk}} = 1$  MeV and  $\Gamma_b = 10^{2.9}$ ) and ( $L_{\gamma, \text{iso}} = 10^{52}$  erg/s,  $\delta t = 0.1$  s and  $\epsilon_{\gamma, \text{pk}} = 0.5$  MeV and  $\Gamma_b = 10^{2.7}$ ). These correspond to a case when the primary spectrum escaping from the GRB fireball is optically thin to photons of all energies, and a case when the primary fireball escaping spectrum is optically thick to  $\gamma\gamma$  against its own photons in a band of photon energies, shown in Figures 4 and 5 respectively. The prompt primary spectra, using equation (18) multiplied by  $\exp[-\tau_{\gamma\gamma, \text{bkg}}(\epsilon_\gamma)]$  to allow for attenuation in the background radiation fields, are plotted as the dark solid curves in both figures. We have also plotted the first generation delayed spectra from IC scattering of secondary leptons on the CMB, by numerically integrating equation (22) for two different IGM magnetic field strengths ( $B_{\text{IG}}$ ) of  $10^{-20}$  G and  $10^{-17}$  G. For the same two sets of parameters above these are given by the dashed and dotted curves respectively. The delayed spectra for 50 s duration (topmost dashed and dotted curves) corresponds to the GRB duration ( $t_{\text{grb}}$ ) and we have calculated them using the full range of secondary pair energy  $\gamma_e = \epsilon_\gamma / 2m_e$ , created with CMB, allowed by the maximum primary photon energy  $\epsilon_\gamma \approx \gamma'_{e, \text{max}} m_e \Gamma_b$  from equation (6). We have also calculated the delayed spectra for  $10^2$ ,  $10^4$

and  $10^6$  s duration by numerically integrating equation (22) up to a maximum  $\gamma_e$  corresponding to that time from Figure 3.

## 5. Discussion

We have calculated the spectrum and time dependence of the high energy ( $\gtrsim$  GeV) spectrum emerging from GRB internal shocks as a function of the luminosity, time variability and the bulk Lorentz factor, using exact cross sections. For typical bursts parameters the internal shock spectrum cuts off above a threshold energy  $E_{\gamma,\text{th}} \sim 10 - 100$  GeV due to  $\gamma\gamma$  interactions within the shock region. There is a qualitative difference with the results of Baring & Harding (1997), who discussed the  $\gamma\gamma$  absorption in external shocks, and who did not consider the secondary spectra from interactions with background radiation. More recently Wang et al. (2004) also discussed the  $\gamma\gamma$  absorption in external shocks, including interactions against background photons. The main difference with our work is due to the much lower  $\gamma\gamma$  optical depth from the lower photon density at the radii of external shocks, which are much larger than the radii of internal shocks considered here. Internal shock  $\gamma\gamma$  absorption using approximate cross sections was discussed by Pilla & Loeb (1998) and Lithwick & Sari (2001) without interactions against external background photons, and by Dai & Lu (2002) including such interactions. These authors did not consider the effects of synchrotron self-absorption. The main qualitative difference between the emerging internal shock spectra of these authors and our work arises from our use of accurate cross sections, and more importantly, our inclusion of synchrotron self-absorption. The cut-offs in the emerging spectra that we obtain are compatible with more detailed numerical calculations of the self-consistent pair creation and annihilation spectrum in internal shocks of Pe’er & Waxman (2003), without inclusion of interactions against external background photons. The main difference between their final spectra and ours is due to their using an ab-initio spectrum instead of a phenomenological Band spectrum as here, and to the additional effects of our inclusion here of interactions against external photons, leading to a delayed secondary spectrum.

A new feature discussed in this paper is that the spectra that emerge from the GRB internal shock region shows, besides the expected high energy cutoff due to pair-production  $E_{\gamma,\text{th}}$ , also a re-emergence of the spectrum at a higher energy  $E_{\gamma,\text{thin}} > E_{\gamma,\text{th}}$  where the shock becomes optically thin again to  $\gamma\gamma$  interactions. This is due to our inclusion of synchrotron self-absorption, which reduces the internal photon target spectral density causing absorption of the highest energy emerging photons. For high enough bulk Lorentz factors (typically  $\Gamma_b \gtrsim 800$ ), the fireball is optically thin to internal  $\gamma\gamma$  interactions at all energies, and there is no internal  $\gamma\gamma$  cut-off band in the emerging spectrum.

The emerging GRB spectrum is modified, on its way to the observer, by interactions with the diffuse infrared background (CIB) and the diffuse microwave background (CMB). Here, we have used the GRB internal shock emerging spectra including synchrotron self-absorption as the source of input photons, and calculate their interaction with a CIB spectrum redshifted to  $z \sim 1$ , based

on that of Malkan & Stecker (2001). We then calculated the secondary GRB spectrum from the resulting secondary pairs which are up-scattered on CMB photons. We used two different escaping GRB primary spectra, one with an internal  $\gamma\gamma$  cutoff band (for a typical burst bulk Lorentz factor  $\Gamma_b \sim 300$ ) and one without an internal  $\gamma\gamma$  cutoff band (for a burst with a larger  $\Gamma_b \sim 800$ ). We used two different isotropic-equivalent luminosities, and different intergalactic magnetic field strengths ranging between  $B_{IG} = 10^{-20}$  G and  $10^{-17}$  G. This leads to a secondary spectrum, mainly in the 1-100 GeV range, in addition to and delayed respect to the prompt unabsorbed internal shock spectrum. We also calculated the further interaction of the secondary gamma-ray spectrum with the CIB, which gives a similarly attenuated spectral shape as that of the primary spectrum. We did not consider the delayed spectrum of the tertiary and higher order pairs, since the delay time scales are longer and the fluxes of these components is much lower.

A different delayed GeV component can arise in the afterglow phase, when the inverse Compton spectrum peak energy in the external shock region sweeps across the GeV band (Mészáros & Rees 1994; Dermer et al. 2000; Sari & Esin 2001; Zhang & Mészáros 2001). This delayed GeV emission, from IC upscattering on external shock electrons, is predicted to be detectable by GLAST at  $z \sim 1$  (Zhang & Mészáros 2001), as long as the shock parameters are such that the IC component is prominent (which is the case for the typical parameters inferred from broadband modeling of some well-studied bursts). The IC duration can be up to a few hours, which could overlap with the earlier part of the delayed spectra discussed here. The temporal evolution of the IC spectral component is such that it hardens with time initially, but softens with time after the IC peak crosses the band. The delayed GeV component discussed in this paper has a rather different temporal evolution behavior. Since  $\Delta t(\gamma_e)$  is essentially anti-correlated with  $\gamma_e$  (see Figure 3), the hard spectrum (due to the more energetic electrons) lasts a shorter timescale than the soft spectrum. Also the harder photons arrive earlier than the softer photons. Throughout the whole delayed phase, the hardest photons emerge first, followed by progressively softer photons. Later the hardest photons drop out first from the spectrum. The delayed spectrum always progressively softens with time. This distinct spectral evolution behavior can be used to distinguish the delayed emission from IC scattering in external shocks from the delayed emission of secondary spectra due to pair-production and IC scattering on the diffuse background discussed here. The secondary external spectrum from such an IC spectrum, however, should be similar to what we have discussed here, on timescales longer than a few hours, since the absorbed energy undergoes similar reprocessing.

The time delays and the flux level of the secondary spectra are sensitive to the intergalactic magnetic field strength. The best prospects for detection of such secondary delayed GeV spectra occurs for bursts with bulk Lorentz factors  $\gtrsim 800$  and intergalactic magnetic fields  $\lesssim 10^{-17}$  G, which might be typical of intergalactic void regions. Since the mean-free-path of the first generation high energy photons against  $\gamma\gamma$  absorption typically exceeds several to tens of Mpc (Coppi & Aharonian 1997; Malkan & Stecker 2001), it is plausible that a substantial fraction of the pair formation will occur in void regions near the burst, even if the latter occurred in a cluster galaxy. The corresponding time delays are in the range 10-100 s and the fluxes are within the sensitivity range of GLAST, and

at the high energy end, also of VERITAS, HEGRA, and other ACTs. A detection of this secondary delayed GeV spectrum in GRB would provide a valuable diagnostic for the IGM magnetic field strength, as well as the bulk Lorentz factor, and would provide valuable clues for the typical size of the shocks responsible for the radiation.

This research is supported in part by NSF AST 0098416, NASA NAG5-13286 and the Monell Foundation.

## REFERENCES

- Band, D., et al. 1993, *ApJ*, 413, 281
- Baring, M. G. & Harding, A. K. 1997, *ApJ*, 491, 663
- Blumenthal, G.R. & Gould, R.J. 1970, *Rev. Mod. Phys.*, 42, 237
- Coppi, P.S. & Aharonian, F.A. 1997, *ApJ*, 487, L9
- Dai, Z.G. & Lu, T. 2002, *ApJ*, 580, 1013
- Dai, Z.G., Zhang, B., Gou, L.J., Mészáros, P. & Waxman, E. 2002, *ApJ*, 580, L7
- Dermer, C.D., Chiang, J. & Mitman, K. 2000, *ApJ*, 537, 785
- Dingus, B.L. 2003, *AIP Conf. Procs.* 662, pp. 240-243
- Fishman, G. K. & Meegan, C. A. 1995, *ARAA*, 33, 415
- Gehrels, N. & Michelson, P. 1999, *AstroParticle Phys.*, 11, 277
- Jauch, J.M. & Rohrlich, F. 1955, in *The theory of photons and electrons* (Addison-Wesley)
- Lithwick, Y. & Sari, R. 2001, *ApJ*, 555, 540
- Malkan, M.A. & Stecker, F.W. 2001, *ApJ*, 555, 641
- Mészáros, P. & Rees, M. J. 1994, *MNRAS*, 269, L41
- Pe’er, A & Waxman, E. 2003, *astro-ph/0311252*
- Pilla, R.P. & Loeb, A. 1998, *ApJ*, 494, L167
- Plaga, R. 1995, *Nature*, 374, 430
- Salamon, M.H. & Stecker, F.W. 1998, *ApJ*, 493, 547
- Sari, R. & Esin, A. 2001, *ApJ*, 548, 787

Wang, X.Y., Cheng, K.S., Dai, Z.G. & Lu, T. 2004, *ApJ*, 604, 306.

Weekes, T. 2000. In: Aharonian, F., Völk, H. (eds), Heidelberg 2000, High Energy Gamma-ray Astronomy. In: *AIP Conf. Proc.*, 558. AIP, NY, p15

Zhang, B. & Mészáros, P. 2001, *ApJ*, 559, 110

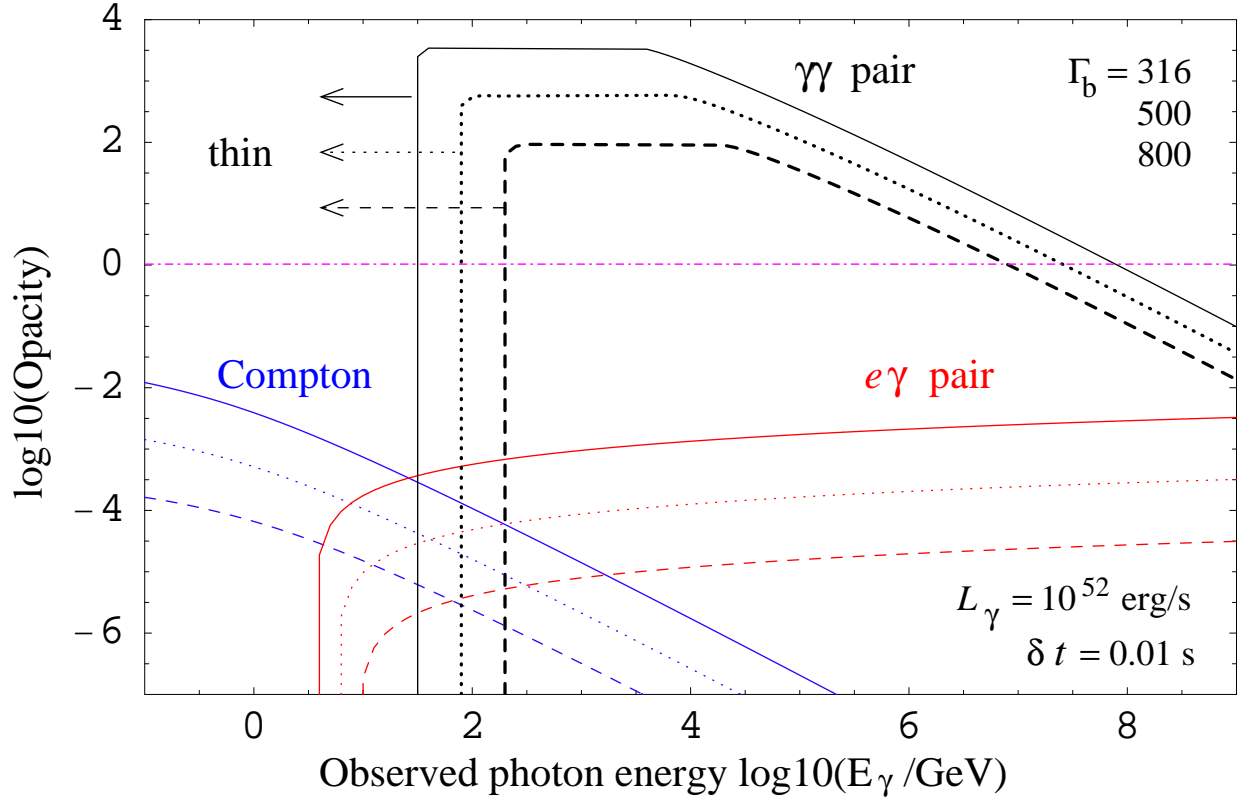


Fig. 1.— Opacity for high energy photons in the GRB fireball, in the comoving frame, against electron Compton scattering,  $e^\pm$  pair production with electrons by  $e\gamma$  and by  $\gamma\gamma$  interactions with fireball photons. We have plotted the curves for  $L_{\gamma,\text{iso}} = 10^{52}$  erg/s isotropic  $\gamma$ -ray luminosity, the bulk Lorentz factor  $\Gamma_b = 316$  (solid curves), 500 (dotted curves) and 800 (dashed curves). We used a variability time  $\delta t = 0.01$  s. Photons above  $\sim 2 \times 10^7$  GeV, for example, for  $\Gamma_b = 316$  will escape the GRB fireball. No photons, for the same parameters, may escape the fireball below  $\sim 2 \times 10^7$  GeV down to  $\sim 26$  GeV where the  $\gamma\gamma$  opacity is greater than unity.

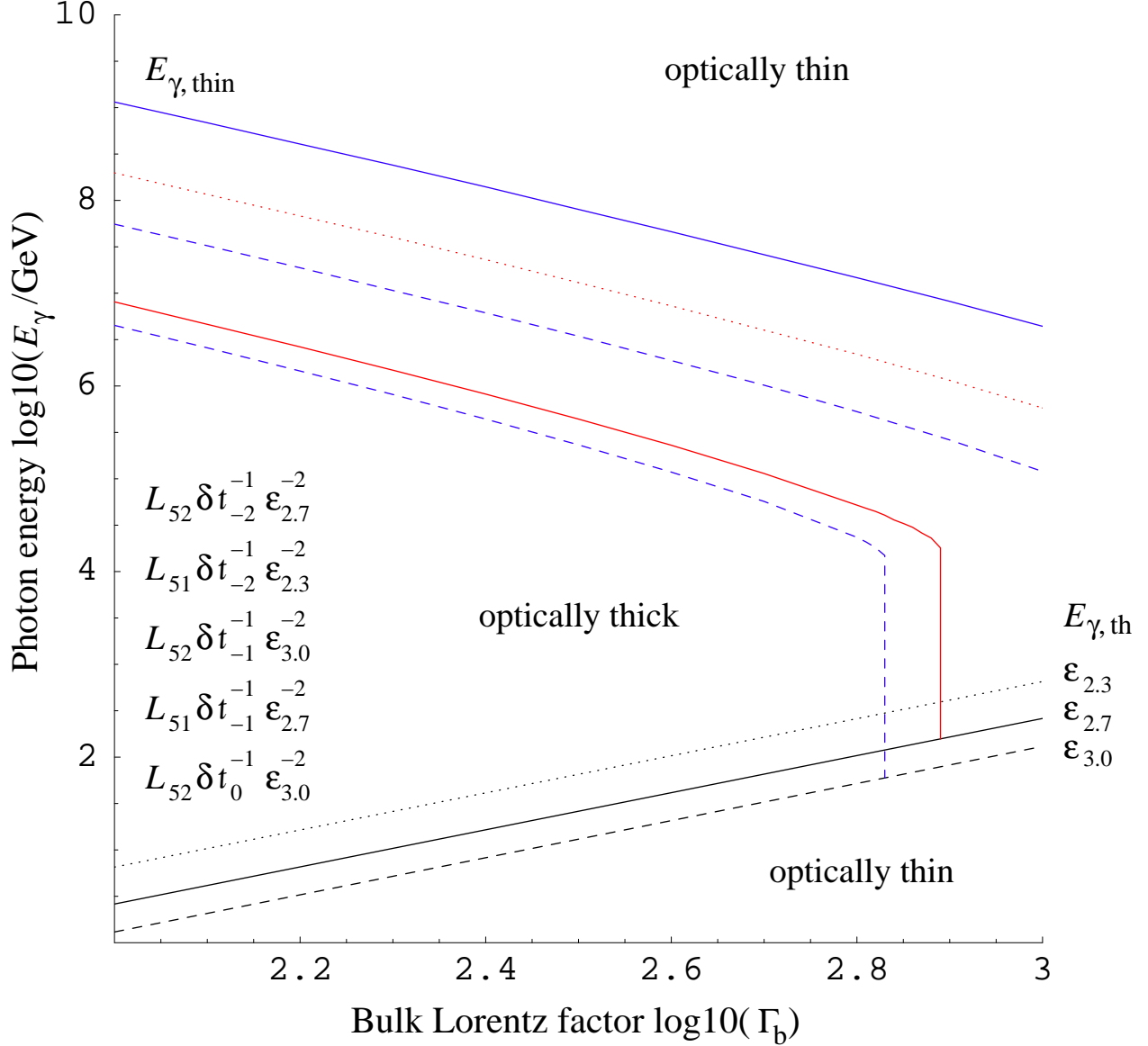


Fig. 2.— Cartoon of allowed (optically thin) and forbidden (optically thick) photon energy range, in the observer’s frame, from the GRB fireball as a function of the bulk Lorentz factor ( $\Gamma_b$ ). Photons below  $E_{\gamma, \text{th}}$  and above  $E_{\gamma, \text{thin}}$  may escape. We have plotted the curves for 2 different  $\gamma$ -ray luminosity  $10^{52}L_{52}$ ,  $10^{51}L_{51}$ ; 4 different variability time  $1\delta t_0$  s,  $0.1\delta t_{-1}$  s,  $0.01\delta t_{-2}$  s,  $0.001\delta t_{-3}$  s; and 3 different peak synchrotron photon energy  $200\epsilon_{2.3}$  keV,  $500\epsilon_{2.7}$  keV,  $1000\epsilon_{3.0}$  keV. However, we have kept the synchrotron self-absorption energy to be fixed at 10 keV in all cases. The parameter choices are shown for curves from top to bottom.

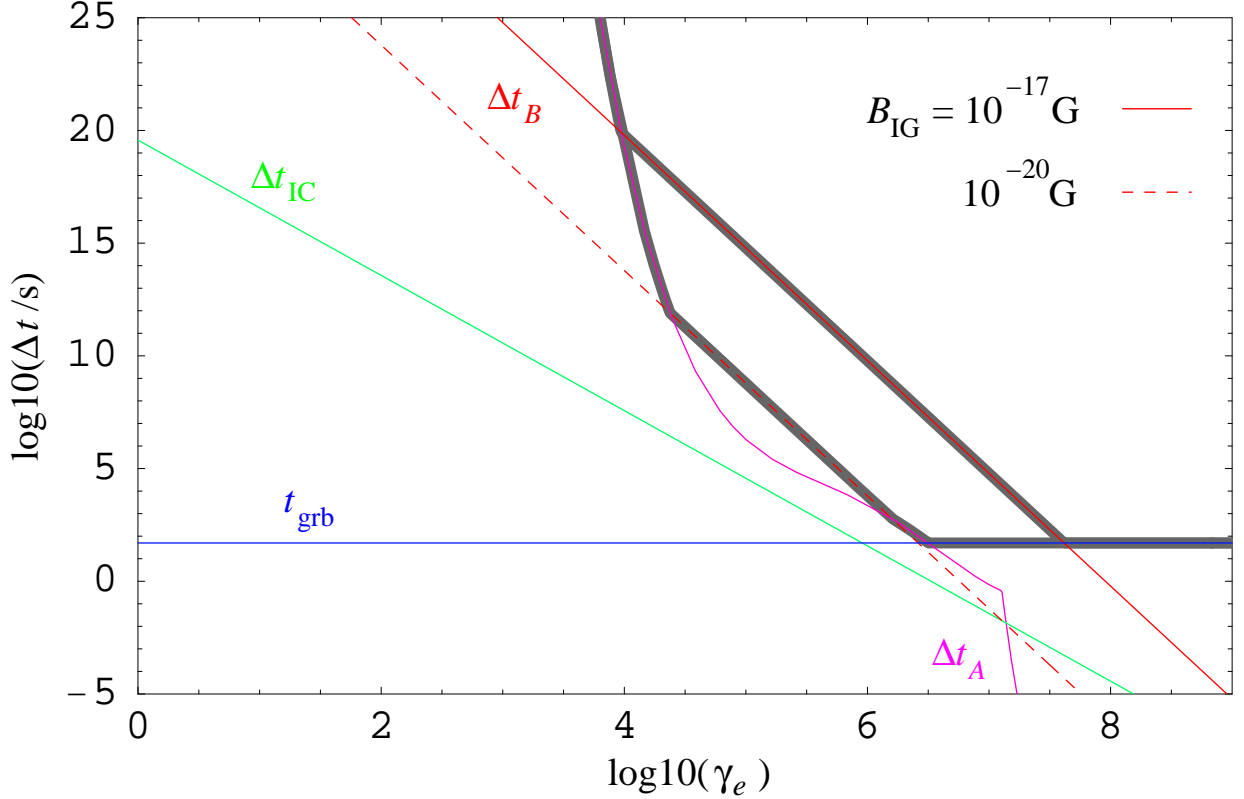


Fig. 3.— Different time scales ( $\Delta t_{\text{IC}}$ ,  $\Delta t_A$ ,  $\Delta t_B$ , and  $t_{\text{grb}}$ ), involved in calculating the delayed secondary IC spectrum using equation (22), as a function of secondary  $e^\pm$  pair energy ( $\gamma_e$ ). The thick gray lines correspond to  $\Delta t(\gamma_e) = \max\{\Delta t_{\text{IC}}, \Delta t_A, \Delta t_B, \delta t\}$  for two different  $\Delta t_B$ , denoted by solid and dashed lines, corresponding to inter-galactic magnetic field strength ( $B_{\text{IG}}$ ) of  $10^{-17}$  and  $10^{-20}$  G respectively. We have used a GRB duration of  $t_{\text{grb}} = 50$  s. All times are plotted for a fixed luminosity distance of  $D_L = 10^{28}$  cm.

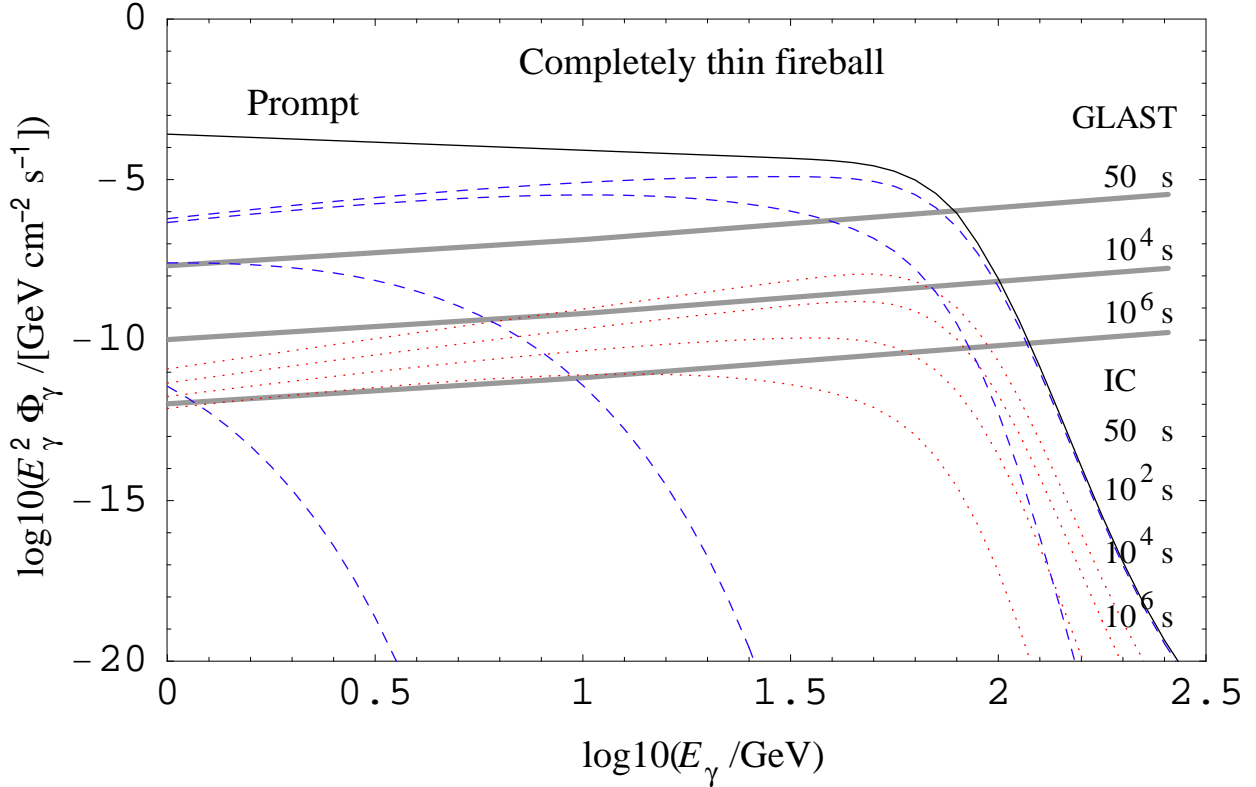


Fig. 4.— High energy photon spectrum ( $E_\gamma^2 \Phi_\gamma = E_\gamma^2 d^2 N_\gamma / dt dE_\gamma$ ) from a GRB where the fireball is  $\gamma\gamma$  optically thin to photons of all energy. The primary spectrum (full line) is due internal shocks, the secondary spectrum (dashed and dotted) is due to  $\gamma\gamma$  interactions and IC scattering in the external environment. The parameters are  $\delta t = 1$  s,  $\epsilon_{\gamma,\text{pk}} = 1$  MeV,  $\Gamma_b = 10^{2.9}$ , isotropic-equivalent luminosity  $10^{52}$  erg/s, spectral index  $\alpha = 2.5$ , located at redshift  $z = 1$ . The delayed spectra are calculated for two different intergalactic magnetic field values,  $B_{\text{IG}} = 10^{-20}$  and  $10^{-17}$  G, denoted by the dashed and the dotted curves respectively. The duration of the delayed secondary emission (from top to bottom) spectra are 50 s,  $10^2$  s,  $10^4$  s and  $10^6$  s. The GLAST sensitivity (thick gray lines) for 50 s,  $10^4$  s and  $10^6$  s integration time is also plotted for comparison.

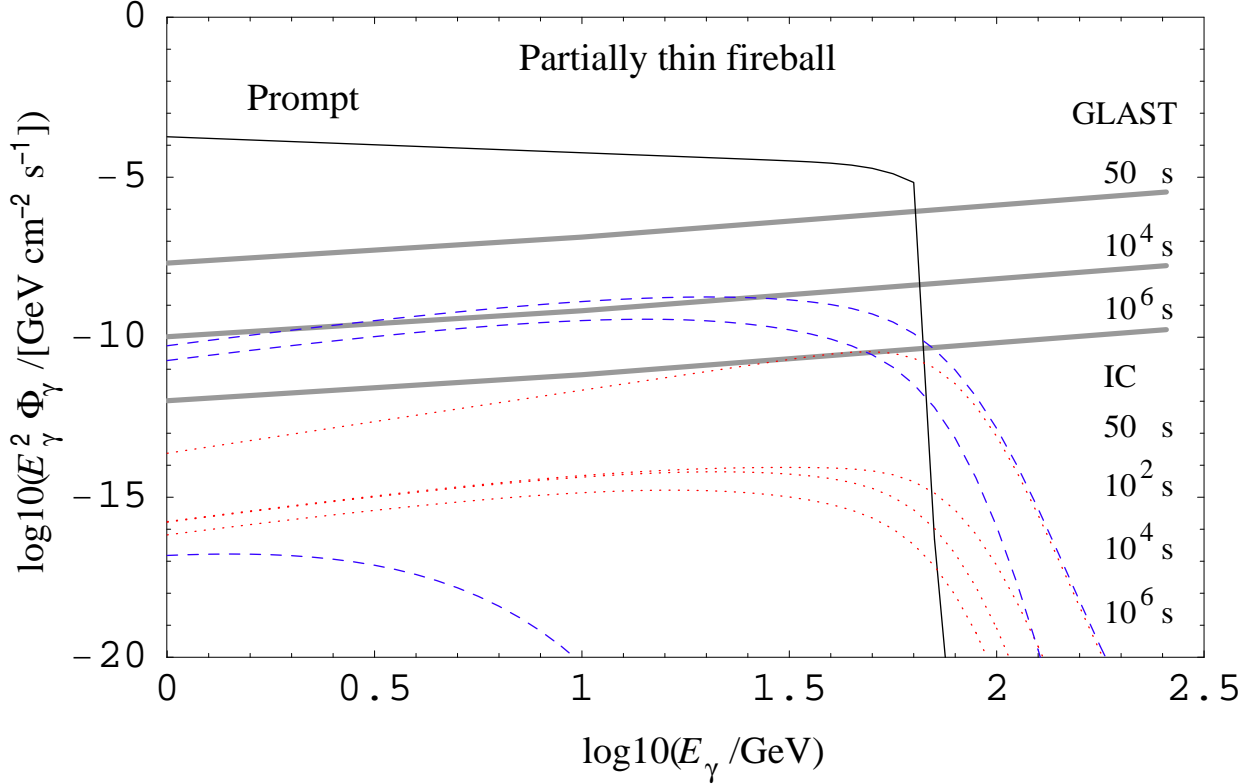


Fig. 5.— High energy photon spectrum ( $E_\gamma^2 \Phi_\gamma = E_\gamma^2 d^2 N_\gamma / dt dE_\gamma$ ) from a GRB where the fireball is optically thick due to  $\gamma\gamma$  against some of its own photons over a certain energy band. The parameters are  $\delta t = 0.1 \text{ s}$ ,  $\epsilon_{\gamma,\text{pk}} = 0.5 \text{ MeV}$ ,  $\Gamma_b = 10^{2.7}$ , isotropic-equivalent luminosity  $10^{52} \text{ erg/s}$ , spectral index  $\alpha = 2.5$ , and redshift  $z = 1$ . Plotted are the prompt (solid curve) and delayed spectra (dashed and dotted curves). The delayed spectra are for two different intergalactic magnetic fields of  $B_{\text{IG}} = 10^{-20}$  and  $10^{-17} \text{ G}$ , denoted by the dashed and the dotted curves respectively. The duration of delayed emission (from top to bottom) spectra are 50 s,  $10^2 \text{ s}$ ,  $10^4 \text{ s}$  and  $10^6 \text{ s}$ . GLAST sensitivities (thick gray lines) for 50 s,  $10^4 \text{ s}$  and  $10^6 \text{ s}$  integration time are also plotted for comparison.